A Model for Film-forming with Newtonian and Shear Thinning Fluids

R W Hewson, N Kapur *and* ***P H Gaskell***

School of Mechanical Engineering, University of Leeds, Leeds. LS2 9JT. UK.

Abstract

The formation of a thin film by (i) the slow penetration of a gas bubble into a liquid filled tube, (ii) the withdrawal of a planar substrate from a liquid filled gap, is investigated theoretically for the cases of both Newtonian and shear thinning liquids; the latter conforming to either a power law or Ellis model. Formulated as a boundary value problem underpinned by lubrication theory, the analysis gives rise to a system of ordinary differential equations which are solved numerically subject to appropriate boundary conditions. For Newtonian liquids comparison of the predicted residual film thickness for a wide range of capillary number, $Ca \in \left(10^{-4}, 10\right)$, is made with others obtained using existing expressions, including the classical one of Bretherton, in the region of parameter space over which they apply. In the case of (i), prediction of the behaviour of the residual fluid fraction and gap-to-film thickness ratio, for a Newtonian liquid and one that is shear-thinning and modelled via a power-law, is found to be in particularly good agreement with experimental data for $Ca < 0.2$. For (ii), both shear thinning models are utilized and contour plots of residual film thickness generated as a function of Ca and the defining parameters characteristic of each model.

1 Introduction

The formation of a continuous thin liquid film, of residual thickness H_∞, directly onto a regular or irregular rigid substrate, following the displacement of one fluid phase (usually a liquid) by a second (normally a gas), occurs both naturally and as part of numerous engineering applications. Examples include: oil extraction in porous media [1]; gas assisted injection molding [2]; a vast array of coated products [3]; the lubrication of machine parts [4]; respiration and the functioning of the lung [5, 6]. In essence, it is a ubiquitous process which depends on one, or a combination, of the following [7, 8]: viscous, surface tension and, at high speed, inertial forces. Not surprisingly, it has attracted a great deal of attention from researchers in an effort to understand and model the problem.

A flow geometry commonly employed for investigating the above involves the formation of a thin film on the inner wall of a smooth circular, liquid filled, tube of radius R by the slow penetration (speed U_b) of a long gas bubble. This has many similarities to the situation encountered in slot and knife coating flows, in which a planar substrate is withdrawn (speed U_s) from a liquid filled gap of width C; the difference being the change of reference from that of a stationary wall and moving gas-liquid interface to one of a stationary interface and moving substrate, see Figure 1.

[Figure 1 here.]

Fairbrother and Stubbs [9] are arguably the first to have investigated the problem experimentally for the case of Newtonian fluids (density ρ, viscosity μ, interfacial surface tension σ), arriving at the following empirical relationship for the residual volume fraction, m, of liquid remaining on the wall of a tube, following displacement

by an air bubble, in terms of capillary number, $Ca = \mu U_c/\sigma$ (ratio of viscous to surface tension forces), where U_c is the appropriate characterisitc velocity, either U_b or U_s:

$$m = \sqrt{Ca}, \quad \text{for} \quad Ca \in \left(0, 1.5 \times 10^{-2}\right), \tag{1}$$

Subsequently, Taylor [10] and Cox [11] undertook similar studies, the upper limit for Ca being 2 and 10, respectively. In addition, Taylor extended the upper range of validity of the Fairbrother & Stubbs' relationship to $Ca = 0.09$. The work of these two authors confirmed Ca to be the dominant factor in determining the residual volume fraction; the latter asymptoting to the value 0.56 (Taylor) and 0.6 (Cox), with increasing Ca. In their experiments, Marchessault and Mason [12] used the electrical resistance of a liquid within a capillary tube to measure the residual volume fraction deposited on the wall of the tube which, for $Ca \in (7 \times 10^{-6}, 2 \times 10^{-4})$, they determined to be proportional to $\sqrt{Ca}$, in agreement with equation (1).

Bretherton [13] investigated the same problem analytically for $Ca \in \left(0, 5 \times 10^{-3}\right)$. Beginning from the lubrication approximation and using the method of matched asymptotic expansions he derived the following relationship for the ratio of the residual film thickness to meniscus radius of curvature, R_C (which, for thin films can be taken as R the tube radius, with $H_\infty/R << 1$):

$$\frac{H_\infty}{R} = 0.643\,(3Ca)^{\frac{2}{3}} = 1.337\,(Ca)^{\frac{2}{3}}, \quad \text{for} \quad Ca \in \left(0, 5 \times 10^{-3}\right); \tag{2}$$

the constant, 0.643, having been obtained numerically.

Schwartz et al. [14] have shown the close relationship between equation (2), and those of Landau-Levich [15] and Frankel [16] for the case of a planar substrate and a soap film, respectively, withdrawn from a bath of liquid, noting the ability of all three to predict reasonably well the asymptotic film thickness for small Ca. See also the more rigorous derivation of the Bretherton expression (including higher order terms) by Park & Homsy [17].

Ruschak [18], on the other hand, investigated the flow in the nip region formed by two rigid, partially submerged, long, horizontally-aligned cylinders, counter-rotating at the same peripheral speed. Using the method of matched asymptotic expansions, it is shown that the first order terms of the inner expansion, close to the point of formation of the meniscus, give rise to the momentum and continuity equations describing the two-dimensional flow there, plus attendant constraints. This free boundary problem was solved numerically using the finite element method and a plot of H_∞/C against $Ca \in (10^{-2}, 10)$ presented, showing good agreement with the classical analysis of Coyne & Elrod [19]. The latter derived a set of ordinary differential equations as a model for the problem of a coated film formed by the withdrawal of a planar substrate from a flooded gap, which they solved numerically, subject to appropriate boundary conditions, for the free surface profile and local meniscus curvature. Their model has since been used extensively to predict the performance of lubrication like geometries with free surfaces present - its capillary number range of applicability, $Ca \in (0, 0.1)$, being greater than that of the Bretherton expression - see for example [20, 21, 22, 23].

From his finite element results, Ruschak suggests an approximate alternative (his equation (5.2)) to equation (2), which he describes as somewhat more useful:

$$\frac{H_\infty}{C} = 0.54\sqrt{Ca} \quad \text{for} \quad Ca \in \left(10^{-2}, 10^{-1}\right). \tag{3}$$

Expressions such as (2) and (3) have been employed when developing simple predictive mathematical models, based on lubrication theory, of forward [24, 25, 26] and reverse [27] roll coating problems, which are seen to compare well with finite element solutions of the corresponding full, two-dimensional free-surface Stokes' problem. The major limitation on their use, however, is that in practice a non-constant meniscus curvature is to be expected for $Ca > 10^{-3}$. An example of this is the reservoir fed rigid roll coating problem investigated by Thompson et al [27]; equation (3) was employed in their lubrication formulation. While comparison with details detailed flow visualisations and corresponding finite element solutions shows that although the film thickness to gap ratio is consistent the shape of the film-forming meniscus is parabolic, rather than circular, thus having a non-constant radius of curvature.

Film forming models in the case of non-Newtonian liquids are less well developed and fewer in number. For shear thinning liquids obeying a power law [28], Weinstein & Ruschak [29], provide the following relationship for predicting the residual film thickness, H_∞, associated with the withdrawal of a substrate from a fluid filled gap:

$$H_\infty = \left[K\left(n\right) R_C\right]^{\frac{3}{2n+1}} \left[\frac{\lambda U_\mathrm{s}}{\sigma}\right]^{\frac{2}{2n+1}}, \quad K\left(n\right) = 2.553e^{-0.65n}, \tag{4}$$

This equation has the same form as that derived by Gutfinger & Tallmadge [30] who, using the method of matched asymptotic expansions, modelled the withdrawal of a shear thinning lubricating film from a bath of liquid. Equation (4) is recovered from that of Gutfinger & Tallmadge by replacing their gravity dependent term with the empirical variable $K\left(n\right)$; λ, is the power law consistency factor; n, the power index; when $n = 1$, that is the fluid is Newtonian, $K = 1.34$ and equation (4) reduces to the classical Bretherton expression, equation (2).

Returning to the problem of residual films formed on the inside wall of a tube, Kamisli & Ryan [31] examined the process for a shear thinning liquid displaced by a finite air bubble forced slowly along its length at a constant speed. As well as conducting detailed experiments, they used the method of matched asymptotic expansions, in much the same way as Bretherton [13], to develop inner and outer solutions, incorporating a power law model. The conclusion they drew was that their approach was inadequate for predicting the film thickness, attributing this to a lack of accuracy when determining the curvature of the bubble. In a subsequent paper [32], they investigated the same problem but this time for the case of a shear thinning liquid displaced by a semi-infinite bubble. The model they developed predicts, qualitatively, that the residual film thickness decreases as the level of shear thinning increases. The main focus of their second paper, however, was the blowout time for open ended tubes (no constriction at the tube exit) and led to an interesting analysis of the velocity of the bubble front along the length of the tube as a function of shear thinning behaviour.

A number of computational studies have been undertaken of free surface flows of visco-elastic fluids (the current analysis is restricted to generalised Newtonian Fluids only - i.e. when the Weissenburg number goes to zero). The visco-elastic nature of the fluid together with the requirement to establish the free surface location as part of the solution make such problems complex. In addition to the conservative equations, the general conformation tensor based constitutive equation must be solved, from which the polymeric contribution to the stress tensor is obtained [33,

34]. Lee et al [35] modelled the planar two dimensional Hele-Shaw free surface problem and were able to capture the decrease in residual film thickness for low fluid elasticities (Weissenberg number) followed by an increase in residual film thickness as the Weissenberg number increases further. The stress boundary layer at the free surface was also resolved and shown to be responsible for thickening of the coating due to the strong positive normal stress gradient in the flow direction leading to a weakening of the recirculating flow upstream of the free surface stagnation point.

Further analysis of visco-elastic fluid flow includes the work of Romero et al. [36] and Bajaj et al. [37] who studied the slot coating of visco-elastic fluids onto a moving substrate as well as the work of Quintella et al. [38] who examined both computationally and experimentally the displacement of a visco-elastic fluid filled capillary tube by a semi-infinite slug of air. This work complements the experimental study of Huzyak and Koelling [39] who undertook an experimental investigation of the penetration of a bubble through a viscoelastic fluid and found that as the fluid becomes more viscoelastic the fractional coverage of fluid left on the tube increases. However this result was found to be highly dependent on the diameter of the tube. The complexity of the computational models for visco-elastic fluids illustrates the need for a simplified model capable of capturing the physics of the fluid film deposition process, one such model was developed by de Ryck and Quéré [40] who used a very elegant lubrication based asymptotic analysis - assuming a Poiseuille velocity profile - to obtain an equation describing the residual fluid film deposited on a wire withdrawn from a fluid filled gap. With only a single adjustable parameter, obtained from experimental data, the analysis provides a useful tool to enable the influence of the different parameters effecting the process to be examined. A similar analysis was undertaken by Ashmore et al. [41] who developed a more general analysis for a range of different geometries in the limits of when the fluid rheology is either dominated by shear thinning effects or elastic effects. In common with the analysis of [40] a quadratic velocity profile is assumed as the constitutive equations lacked an analytical solution. Their model showed excellent qualitative agreement with the experiments they undertook, with quantitative agreement observed for the shear-thinning dominated flows.

This paper revisits the film-forming problem, using lubrication theory to analyse the withdrawal of a planar substrate from a gap filled with a shear thinning liquid, Figure 1(a), whose viscosity follows either a power law or Ellis relationship [42, 43], resulting in a well defined boundary value problem. The associated mathematical model is developed in section 2 in terms of the shear thinning model of choice; described also is the method of solution - section 3. Results follow in section 4, with comparisons made of predictions of residual film thickness for both Newtonian and shear thinning liquids against the experimental data of Kamisli & Ryan [31]; in addition contour plots of residual film thickness generated, using both shear thinning models, as a function of Ca and their characteristic defining parameters, are discussed. Conclusions are drawn in section 5.

2 Mathematical Model

[Figure 2 here.]

Figure 2 defines the flow geometry and coordinate system employed; a local system aligned with the free surface, which is pinned at the tip of the stationary side of the flooded gap, is specified in which the flow is assumed to be perpendicular to it

rather than the rigid planar substrate sweeping liquid from the gap. The steady, inertialess, isothermal flow of an incompressible liquid is governed by the Stokes and continuity equations, namely:

$$\begin{aligned} 0 &= -\nabla P + \nabla\left(\overline{\eta}\nabla\underline{U}\right) \\ 0 &= \nabla\cdot\underline{U}, \end{aligned} \tag{5}$$

where $\overline{\eta}$ and P are the liquid viscosity and pressure, while $\underline{U} = (U, V)$ and $\underline{X} = (X, Y)$ are the velocity and spatial components of the flow, respectively.

Since the solution domain of interest has a length much greater than the surface separation, $H' \in [0, C]$, by invoking the usual lubrication assumptions the above reduce to the following single equation:

$$\frac{dP}{dX} = \frac{d\overline{\tau}}{dY}, \tag{6}$$

where $\overline{\tau} = \overline{\eta}\frac{dU}{dY}$ is the shear stress as a function of the shear rate, $\frac{dU}{dY}$.

As the viscosity of the gas phase can be assumed much less than the liquid phase then, at the free-surface, $Y = 0$, $\overline{\tau} = 0$, and on integrating equation (6) subject to this condition the following equation, describing the shear stress of a generalised Newtonian fluid, is obtained:

$$\overline{\tau} = \frac{dP}{dX}Y. \tag{7}$$

In addition, balancing the pressure discontinuity across the interface and the surface tension forces as given by the Young-Laplace [3] equation gives:

$$P = -\sigma\frac{d\theta}{dX}. \tag{8}$$

Two candidate shear thinning models are considered: (i) the power law [28] due to its simplicity; (ii) the Ellis model [43] which, unlike the former that predicts an infinite viscosity for zero shear stress, includes a finite zero shear viscosity making it generally better suited for the analysis of the free surface problem of interest.

2.1 Power Law Formulation

For a shear thinning liquid which obeys the power law, the shear stress is defined [44] as:

$$\overline{\tau} = \lambda\left|\frac{dU}{dY}\right|^{n-1}\frac{dU}{dY}. \tag{9}$$

Equating the right hand sides of equations (7) and (9) gives, in non-dimensional form:

$$\left|\frac{du}{dy}\right|^{n-1}\frac{du}{dy} = \frac{dp}{dx}y, \tag{10}$$

the following scalings having been employed:

$$u = \frac{U}{U_s}; \quad (x, y, h, h', h_\infty) = \frac{(X, Y, H, H', H_\infty)}{C}; \\ \tau = \frac{\overline{\tau} C^n}{\lambda U_s^n}; \eta = \frac{\overline{\eta} C^{n-1}}{\lambda U_s^{n-1}}; \quad p = \frac{P C^n}{\lambda U_s^n}. \tag{11}$$

From continuity of mass considerations the sign of the pressure gradient is positive, that is when $h \geq 1$ then $\frac{dp}{dx} \geq 0$. As $y \leq h$ the equation describing the velocity gradient, equation (10), becomes:

$$\frac{du}{dy} = \left(\frac{dp}{dx} y\right)^{\frac{1}{n}}, \tag{12}$$

which can be integrated with respect to y to obtain the velocity profile perpendicular to the free surface, noting that at $y = h$ (the planar moving substrate) the velocity $u(y = h) = \cos\theta$, giving:

$$u = \cos\theta + \frac{\left(\frac{dp}{dx} y\right)^{\frac{1}{n}} ny - \left(\frac{dp}{dx} h\right)^{\frac{1}{n}} nh}{n + 1}. \tag{13}$$

The dimensionless flux, q, is obtained by integrating equation (13) from $y = 0$ to h, leading to the following expression for the pressure gradient:

$$\frac{dp}{dx} = \left(\frac{(2n + 1)(h\cos\theta - q)}{n h^{\frac{2n+1}{n}}}\right)^n. \tag{14}$$

Conservation of mass dictates that:

$$\frac{dq}{dx} = 0, \tag{15}$$

while the following geometric relationships hold:

$$\frac{dh'}{dx} = \sin\theta, \tag{16}$$

$$\frac{dx'}{dx} = \cos\theta. \tag{17}$$

Non-dimensionalising equation (8) according to (11) gives:

$$p = -\frac{1}{Ca_P}\frac{d\theta}{dx}; \quad \text{with} \quad Ca_P = \frac{\lambda U_s^n}{\sigma C^{n-1}}. \tag{18}$$

Substituting for the pressure gradient given by equation (14) into the velocity equation, equation (13), gives the location of the free surface stagnation point, $u = 0$ at $y = 0$, as:

$$h = \frac{2n + 1}{n\cos\theta} q, \tag{19}$$

the corresponding film thickness, $h' = hcos\theta$, at which the stagnation point is lo-

cated, being:

$$h' = \frac{2n+1}{n} q. \tag{20}$$

This result is in clear agreement with the film thickness at the stagnation point as predicted by the Coyne & Elrod model for Newtonian liquids; indeed plotting h'/q as a function of n reveals a smooth monotonic transition to the value of 3 at $n = 1$.

2.2 Ellis Fluid Formulation

Unlike the power law, which relates shear rate and viscosity, the Ellis model relates shear stress and viscosity as follows:

$$\eta = \frac{1}{1 + \left| \frac{\tau}{\tau_{\frac{1}{2}}} \right|^{\alpha-1}}, \tag{21}$$

based on the following non-dimensional scalings for P, $\overline{\tau}$ and $\overline{\eta}$, together with those for U, X, Y, H, H', H_∞ as per (11):

$$p = \frac{PC}{\overline{\eta}_0 U_\mathrm{s}}; \quad \tau = \frac{C\overline{\tau}}{\overline{\eta}_0 U_\mathrm{s}}; \quad \eta = \frac{\overline{\eta}}{\overline{\eta}_0}; \tag{22}$$

where $\overline{\eta}_0$ is the viscosity at zero shear stress, $\overline{\tau}_{\frac{1}{2}}$ is the characteristic shear stress and α is analogous to the reciprocal of the power index n in the power law model. Multiplying both sides of equation (21) by the shear rate and rearranging, gives shear rate as a function of shear stress:

$$\tau + \tau \left| \frac{\tau}{\tau_{\frac{1}{2}}} \right|^{\alpha-1} = \frac{du}{dy}. \tag{23}$$

Non-dimensionalising Equation (7) using the scalings given by (22), and substituting for τ in equation (23) gives:

$$\frac{du}{dy} = \frac{dp}{dx} y + \frac{1}{\tau_{\frac{1}{2}}^{\alpha-1}} \left(\frac{dp}{dx} y \right) \left| \frac{dp}{dx} y \right|^{\alpha-1}. \tag{24}$$

Integrating equation (24) with respect to y, and applying the boundary condition $u = \cos\theta$ at $y = h$, leads to:

$$u = \frac{\left(\left(\frac{dp}{dx} y \right)^{\alpha+1} - \left(\frac{dp}{dx} h \right)^{\alpha+1} \right) {\tau_{\frac{1}{2}}}^{1-\alpha}}{\frac{dp}{dx} (\alpha+1)} + \left(\cos\theta + \frac{1}{2} \left(y^2 - h^2 \right) \frac{dp}{dx} \right). \tag{25}$$

Integrating the above again, from $y = 0$ to $y = h$, results in the following relationship between the flux and the pressure gradient:

$$q = \frac{-3{\tau_{\frac{1}{2}}}^{(1-\alpha)} h^{(\alpha+2)} {\frac{dp}{dx}}^{\alpha} - h \left(\frac{dp}{dx} h^2 - 3\cos\theta \right) (\alpha+2)}{3\alpha + 6} \tag{26}$$

Non-dimensionalising equation (8) gives:

$$p = -\frac{1}{Ca_E}\frac{d\theta}{dx}; \quad \text{with} \quad Ca_E = \frac{U_s\overline{\eta}_0}{\sigma}. \tag{27}$$

2.3 Boundary Conditions

Five boundary conditions are required to close the problem. These are:

$$p_{x\to\infty} = 0, \tag{28}$$
$$h_{x=0} = 1, \tag{29}$$
$$x'_{x=0} = 0, \tag{30}$$
$$\theta_{x=0} = -\frac{\pi}{2}, \tag{31}$$
$$h_{x\to\infty} = q. \tag{32}$$

Condition (31) can be replaced with $q_{x=1} = q$, where q is the volume flow rate, if the contact angle, made with the stationary wall forming the gap - see Figure 2. - is unspecified but the final film thickness is known. This boundary condition would be applied in situations where the meniscus is pinned, as is often encountered in blade coating.

3 Method of Solution

The five first-order ordinary differential equations (15) to (17) and either (i) (14) and (18) for power law or (ii) (26) and (32) for Ellis fluids together with the constraint $h' = hcos\theta$ were solved, subject to the boundary conditions (28) to (32) - using the BVP4c solver which forms part of the MATLAB suite of software tools.

Using continuation (progressively decreasing the error) leads to a stable calculation procedure with, for power-law liquids, individual data points being calculated in less than three minutes. The latter time is greatly reduced when generating successive data values using the previous solution as an initial guess. The only significant difference in generating solutions for an Ellis liquid is that the pressure field has to be solved iteratively. The iterative approach adopted makes use of Newton's method by writing:

$$\left.\frac{dp}{dx}\right|_{i+1} = \left.\frac{dp}{dx}\right|_{i} - \frac{g\left(\left.\frac{dp}{dx}\right|_i\right)}{g'\left(\left.\frac{dp}{dx}\right|_i\right)}, \tag{33}$$

where $i+1$ and i denote the value of the pressure gradient between successive iteration steps and, from equation (26):

$$g\left(\frac{dp}{dx}\right) = \frac{-3\tau_{\frac{1}{2}}{}^{(1-\alpha)}h^{(\alpha+2)}\frac{dp}{dx}{}^{\alpha} - h\left(\frac{dp}{dx}h^2 - 3\cos\theta\right)(\alpha+2)}{3\alpha+6} - q, \tag{34}$$

with $g'\left(\frac{dp}{dx}\right)$ being the derivative of $g\left(\frac{dp}{dx}\right)$ with respect to $\frac{dp}{dx}$. By applying Newton's method the pressure gradient equation to be solved is:

$$\left.\frac{dp}{dx}\right|_{i+1} = \frac{3h^{\alpha+2}\left(\left.\frac{dp}{dx}\right|_i^{\alpha}\alpha - \left.\frac{dp}{dx}\right|_i^{\alpha}\right)\tau_{\frac{1}{2}}{}^{1-\alpha} + 3\left(\alpha+2\right)\left(h\cos\theta - q\right)}{3\tau_{\frac{1}{2}}{}^{1-\alpha}h^{\alpha+2}\left.\frac{dp}{dx}\right|_i^{\alpha-1}\alpha + h^3\left(\alpha+2\right)} \tag{35}$$

An initial guess for the pressure gradient is obtained by putting $\alpha = 1$ into equation (26), which describes the Newtonian case, and rearranging, namely:

$$\frac{dp}{dx} = \frac{3\left(h\cos\theta - q\right)}{2h^3}. \tag{36}$$

Accordingly each continuation step uses the pressure field from the previous solution as the starting point for the next, the first such iterative solution being generated from the pressure field given by equation (36). Convergence was ensured by iterating until the difference between successive solutions was less than 10^{-10}.

Note that the pressure gradient when $\alpha = 1$ given by equation (36) is half that obtained via equation (14) for a power law liquid when $n = 1$. This is due to the dimensionless viscosity as obtained by the Ellis model being $\eta = 0.5$ as opposed to $\eta = 1$ for the power law model.

4 Results

Before considering the shear thinning results, those obtained for Newtonian fluids are compared. Figure 3 is a plot of h_∞ against $Ca \in \left(10^{-4}, 10\right)$ comparing results from the boundary value problem (BVP) derived here with those for the models of: Bretherton, $Ca \in (0, 0.01)$; Ruschak, $Ca \in (0.01, 0.1)$; Coyne & Elrod (CE), $Ca \in \left(10^{-4}, 10\right)$. In all cases agreement is found to be extremely good; that between the BVP and CE results being particularly so over the entire Ca range considered.

Figure 4 compares the radius of curvature (non-dimensionalised with respect to $C - H_\infty$ rather than C) at the point at which $\theta = 90°$, showing that as Ca increases both the BVP and CE solutions predict a decrease in radius of curvature, the extent of which differs, with the latter predicting a much larger decrease. The CE results predict that for large Ca the local radius of curvature appears to tend to zero, whereas the BVP ones suggest that although there is a decrease in local radius of curvature, as is to be expected due to the increased viscous forces, this is much more gradual. Both the Bretherton and the Ruschak models result in a radius of curvature that is unity for all Ca, since they assume a constant radius of curvature, which is a reasonable assumption at low $Ca(< 10^{-3})$ only.

[Figure 3 here.]

[Figure 4 here.]

4.1 Power Law Liquids

Figure 5 shows a typical film forming solution obtained with the BVP formulation for a shear thinning liquid, in this case with $n = 0.75$ and $Ca_p = 0.005$. The location of the free surface stagnation point is clearly identifiable. The plot also shows how the pressure recovers monotonically from being subambient at $x = 0$ to a downstream reference value of zero beyond $x = 1.5$. Similarly, the free surface

velocity is negative between $x = 0$ and the free surface stagnation point, beyond which it increases monotonically to the value 1.0 for $x > 1.5$.

[Figure 5 here.]

Predictions for the formation of a thin fluid film in the case if both a Newtonian and a shear-thinning liquid, are compared with complementary experimental data obtained by Kamisli & Ryan [31] (KR) for the case of liquid displaced by the motion of a semi-infinite bubble through a liquid filled tube. As such, figures 6 and 7 show plots of residual fluid fraction and gap to film thickness ratios, respectively, against $Ca_P \in (0, 1)$.

Note that, from the geometry, the film thickness formed, h_∞, according to the solution of the BVP is is related to the residual fluid fraction, m, deposited on the tube wall by the following equation:

$$m = \frac{\pi - \pi \left(1 - h_\infty\right)^2}{\pi} = 2h_\infty \left(1 - h_\infty\right). \tag{37}$$

[Figure 6 here.]

[Figure 7 here.]

It can be seen that, for $Ca_P < 0.5$, the effect of decreasing power index (increasing shear thinning) leads to a reduction in the final film thickness (or fluid deposited) and a corresponding increase in gap to film thickness ratio. Agreement is particularly good in both cases for $Ca_P < 0.2$. While it would be expected that as the capillary number increases the agreement with the experimental results breaks down for both Newtonian and shear thinning fluids it is interesting to see that this break down occurs at lower capillary numbers for shear thinning fluids than it does for the Newtonian case. It is proposed that the reason for this is that in the low shear rate region (such as the region of recirculating flow) the power law model predicts unrealistically high viscosities; as the capillary number increases these regions play a greater role in determining the free surface profile. It is interesting to note that shear thinning leads to an apparently greater asymptotic limit of residual fluid fraction, this is consistent with the experimental work of Gauri & Koelling [45] who studied the motion of bubbles through viscoelastic fluids, which exhibited shear thinning, in capillary tubes.

Figure 8 is a contour plot for the residual film thickness in terms of the power index n, plotted vertically, against Ca_P. It is shown that for all values of Ca_P the residual film thickness decreases as the liquid becomes more shear thinning (i.e. decreasing n). However, care should be exercised with this interpretation in its strictest sense since the nature of the power law is such that Ca_p is a function of both C and n; the two parameters plotted in this figure are, therefore, not truly independent of each other.

[Figure 8 here.]

4.2 Ellis Liquids

The BVP predictions obtained for an Ellis liquid are shown as two sets of contour plots for the residual film thickness: firstly, for $\tau_{\frac{1}{2}}$ against Ca_E for three values

of α (note that for the case $\alpha = 1$ the fluid is Newtonian and the film thickness is therefore independent of $\tau_{\frac{1}{2}}$); secondly, for $\tau_{\frac{1}{2}}$ against α for three values of Ca_E. Figure 9 reveals that an increase in Ca_E, with $\tau_{\frac{1}{2}}$ fixed, leads to a rise in residual film thickness; this is as expected and is in agreement with the Newtonian based theory of Bretherton. It can also be observed that for $\alpha > 1$, as $\tau_{\frac{1}{2}}$ increases with Ca_E fixed, the residual film thickness increases, the effect becoming more significant as the level of shear thinning, α, increases. The reason for this is that as $\tau_{\frac{1}{2}}$ decreases the fluid viscosity decreases (for a given Ca_E and α, see equation (21)), leading to lower viscous forces and a smaller film thickness. From Figure 10 the effect of changing $\tau_{\frac{1}{2}}$, at a fixed value of α, can clearly be seen to increase the residual film thickness; the level of increase becoming more pronounced with an increase in shear thinning. For a capillary number of $Ca_E = 1$, a decrease in residual film thickness with increasing α is observed for $\tau_{\frac{1}{2}} \gtrapprox 0.5$. Caution must be applied when considering this result as the capillary number examined is large and is likely to be around the limit of applicability of the model.

[Figure 9 here.]

[Figure 10 here.]

Note that although in a fluid bulk the Ellis model reduces to the power law model when $\tau >> \tau_{\frac{1}{2}}$, along a free surface the shear stress is zero and the condition $\tau >> \tau_{\frac{1}{2}}$ can not be met there. For this reason the results of the power law model do not converge to those of the Ellis model for decreasing $\tau_{\frac{1}{2}}$.

5 Conclusion

A model for film forming has been derived as a BVP for the case of shear thinning liquids and which holds in the Newtonian limit. Comparison with earlier work, both theoretical and experimental, is made and shown to be in good agreement over a wide range of capillary numbers.

For shear thinning liquids, modelled by a power-law, the agreement between prediction and the experimental data of Kamisli & Ryan [31] is particularly encouraging and provides confidence in relation to applying the new model for the solution of a variety of problems involving shear thinning liquids, including many lubrication and coating flows. However, based on the scant experimental data available for comparison purposes the rather conservative limit of $Ca_P \in (0, 0.2)$ is suggested for which the new model is assumed valid; additional good quality complementary experimental data is needed to assess its true range of applicability.

The work similarly highlights the requirement for new experimental data that can be used to validate the modelling approach in the case of shear-thinning liquids conforming to an Ellis description, the form of which includes a zero shear rate viscosity thus making it more realistic for inclusion in free surface flow analyses.

6 Acknowledgement

The authors wish to thank the reviewers for their insightful comments.

References

[1] J. Stark and M. Manga. The motion of long bubbles in a network of tubes. *Transport in Porous Media*, 40(2):201–218, 2000.

[2] A. Polynkin, J. F. T. Pittman, and J. Sienz. Gas displacing liquids from tubes: high capillary number flow of a power law liquid including inertia effects. *Chemical Engineering Science*, 59(14):2969–2982, 2004.

[3] S. F. Kistler and P. M. Schweizer. *Liquid Film Coating - Scientific Principles And Their Technological Implications*. Chapman and Hall, London, 1997.

[4] A. Cameron. *Basic Lubrication Theory*. Longman, 1979.

[5] J. Rosenzweig and O. E. Jensen. Capillary-elastic instabilities of liquid-lined lung airways. *Journal of Biomechanical Engineering – Transactions of the ASME*, 124(6):650–655, 2002.

[6] J. B. Grotberg and O. E. Jensen. Biofluid mechanics in flexible tubes. *Annual Review of Fluid Mechanics*, 36:121–147, 2004.

[7] D. Quéré. Fluid coating on a fiber. *Annual Review of Fluid Mechanics*, 31:347–384, 1999.

[8] D. Quéré. Fluid coating. In *Proceedings of the 3rd European Coating Symposium - Advances in Coating and Drying of Thin Films*, pages 11–32, Nurenburg, Germany, 1999.

[9] F. Fairbrother and A. E. Stubbs. Studies in electro-endosmosis. part vi. the "bubble-tube" method of measurement. *Journal of Chemistry*, page 527, 1935.

[10] G. I. Taylor. Deposition of a viscous fluid on the wall of a tube. *Journal of Fluid Mechanics*, 10(2):161–165, 1961.

[11] B. G. Cox. On driving a viscous fluid out of a tube. *Journal of Fluid Mechanics*, 14(1):81–96, 1962.

[12] R. N. Marchessault and S. G. Mason. flow of entrapped bubbles through a capillary. *Industrial & Engineering Chemistry*, 52(1):79 – 84, 1960.

[13] F.P. Bretherton. The motion of long bubbles in tubes. *Journal of Fluid Mechanics*, 10:166, 1961.

[14] L. W. Schwartz, H. M. Princen, and A. D. Kiss. On the motion of bubbles in capillary tubes. *Journal of Fluid Mechanics*, 172:259–275, 1986.

[15] L. Landau and B. Levich. Dragging of a liquid by a moving plate. *ACTA Physicochimica URSS*, 17:42, 1942.

[16] J. Lyklema, P. C. Scholten, and K. J. Mysels. Flow in thin liquid films. *Journal of Physical Chemistry*, 69(1):116–123, 1965.

[17] C. W. Park and G. M. Homsy. 2-phase displacement in Hele Shaw cells – theory. *Journal of Fluid Mechanics*, 139(FEB):291–308, 1984.

[18] K. J. Ruschak. Boundary-conditions at a liquid air interface in lubrication flows. *Journal of Fluid Mechanics*, 119(JUN):107–120, 1982.

[19] J. C. Coyne and H. G. Elrod. Conditions for the rupture of a lubricating film. Part 1: Theoretical model. *Journal of Lubrication Technology*, 92:451, 1970.

[20] J. Greener and S. Middleman. Theoretical and experimental studies of the fluid dynamics of a two-roll coater. *Industrial and Engineering Chemistry Fundamentals*, 18(1):35–41, 1979.

[21] H. Benkreira, M. F. Edwards, and W. L. Wilkinson. Ribbing instability in the roll coating of Newtonian fluids. *Plastics and Rubber Processing and Applications*, 2:137–144, 1982.

[22] M. Priest, D. Dowson, and C. M. Taylor. Theoretical modelling of cavitation in piston ring lubrication. *Proceedings of the Institution of Mechanical Engineers Part C- Journal of Mechanical Engineering Science*, 214(3):435–447, 2000.

[23] R. W. Hewson, N. Kapur, and P. H. Gaskell. A theoretical and experimental investigation of tri-helical gravure roll coating. *Chemical Engineering Science*, 61(16):5487–5499, 2006.

[24] P. H. Gaskell, M. D. Savage, J. L. Summers, and H. M. Thompson. Modelling and analysis of meniscus roll coating. *Journal of Fluid Mechanics*, 298:113–137, 1995.

[25] P. H. Gaskell, N. Kapur, and M. D. Savage. Bead-break instability. *Physics of Fluids*, 13(5):1243–1253, 2001.

[26] J. L. Summers, H. M. Thompson, and P. H. Gaskell. Flow structure and transfer jets in a contra-rotating rigid-roll coating system. *Theoretical and Computational Fluid Dynamics*, 17(3):189–212, 2004.

[27] H. M. Thompson, N. Kapur, P. H. Gaskell, J. L. Summers, and S. J. Abbott. A theoretical and experimental investigation of reservoir-fed, rigid-roll coating. *Chemical Engineering Science*, 56(15):4627–4641, 2001.

[28] J. G. Oldroyd. On the formulation of rheological equations of state. *Proceedings of the Royal Society of London Series A – Mathematical and Physical Sciences*, 200(1063):523–541, 1950.

[29] S. J. Weinstein and K. J. Ruschak. Coating rows. *Annual Review of Fluid Mechanics*, 36:29–53, 2004.

[30] C. Gutfinger and J. A. Tallmadge. Films of non-Newtonian fluids adhering to flat plates. *AICHE Journal*, 11:403–413, 1965.

[31] F. Kamisli and M. E. Ryan. Perturbation method in gas-assisted power-law fluid displacement in a circular tube and a rectangular channel. *Chemical Engineering Journal*, 75(3):167–176, 1999.

[32] F. Kamisli and M. E. Ryan. Gas-assisted non-Newtonian fluid displacement in circular tubes and noncircular channels. *Chemical Engineering Science*, 56(16):4913–4928, 2001.

[33] M. Pasquali and L. E. Scriven. Free surface flows of polymer solutions with models based on the conformation tensor. *Journal of Non-Newtonian Fluid Mechanics*, 108(1-3):363–409, 2002.

[34] M. Behr, D. Arora, O. M. Coronado, and M. Pasquali. GLS-type finite element methods for visco-elastic fluid flow simulations. In K.J. Bathe, editor, *Third MIT Conference on Computational Fluid and Solid Mechanics*, pages 586–589, 2005.

[35] A. G. Lee, E. S. G. Shaqfeh, and B. Khomami. A study of viscoelastic free surface flows by the finite element method: Hele-shaw and slot coating flows. *Journal of Non-Newtonian Fluid Mechanics*, 108(1-3):327–362, 2002.

[36] O. J. Romero, L. E. Scriven, and M. S. Carvalho. Slot coating of mildly viscoelastic liquids. *Journal of Non-Newtonian Fluid Mechanics*, 138(2-3):63–75, 2006.

[37] W. Bajaj, J. R. Prakash, and M. Pasquali. A computational study of the effect of viscoelasticity on slot coating flow of dilute polymer solutions. *Journal of Non-Newtonian Fluid Mechanics*, 149(1-3):104–123, 2008.

[38] E. F. Quintella, P. R. S. Mendes, and M. S. Carvalho. Displacement flows of dilute polymer solutions in capillaries. *Journal of Non-Newtonian Fluid Mechanics*, 147:117–128, 2007.

[39] P. C. Huzyak and K. W. Koelling. The penetration of a long bubble through a viscoelastic fluid in a tube. *Journal of Non-Newtonian Fluid Mechanics*, 71(1-2):73–88, 1997.

[40] A. de Ryck and D. Quéré. Fluid coating from a polymer solution. *Langmuir*, 14(7):1911–1914, 1998.

[41] J. Ashmore, A. Q. Shen, H. P. Kavehpour, H. A. Stone, and G. H. McKinley. Coating flows of non-Newtonian fluids: weakly and strongly elastic limits. *Journal of Engineering Mathematics*, 60:17–41, 2008.

[42] M. Reiner. *Deformation, Strain and Flow.* H. K. Lewis & Co. Ltd., London, 2 edition, 1960.

[43] S. Matsuhis and R. B. Bird. Analytical and numerical solutions for laminar flow of non-Newtonian Ellis fluid. *AICHE Journal*, 11(4):588–595, 1965.

[44] R. B. Bird, R. C. Armstrong, and O. Hassager. *Dynamics of Polymeric Liquids*, volume 1. Wiley, New York, 2 edition, 1987.

[45] V. Gauri and K. W. Koelling. The motion of long bubbles through viscoelastic fluids in capillary tubes. *Rheologica Acta*, 38(5):458–470, 1999.

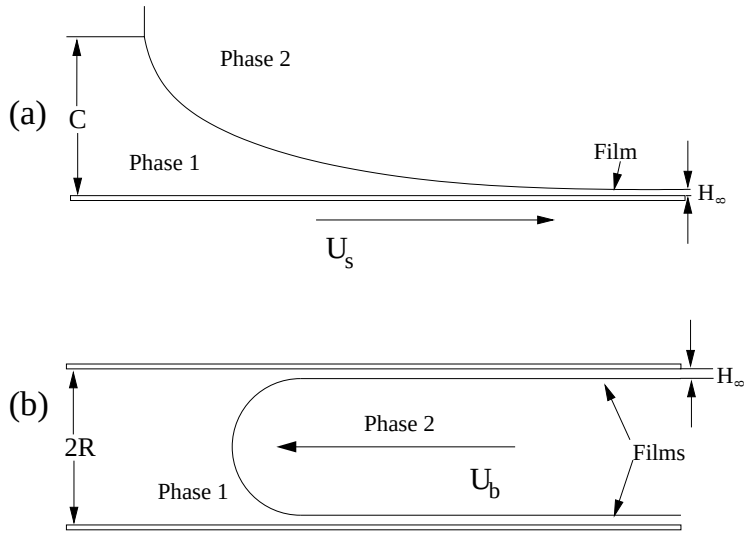

Figure 1: Illustration of the similarity between film forming in the case of: (a) the withdrawal of a planar surface from a liquid filled gap; (b) liquid in a circular tube displaced by a long penetrating gas bubble.

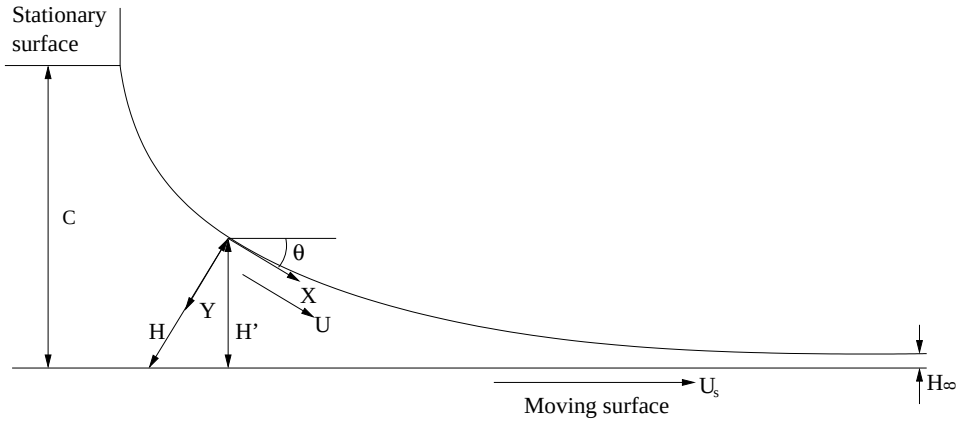

Figure 2: Schematic of the film forming geometry analysed as a boundary value problem, shown also is the coordinate system adopted.

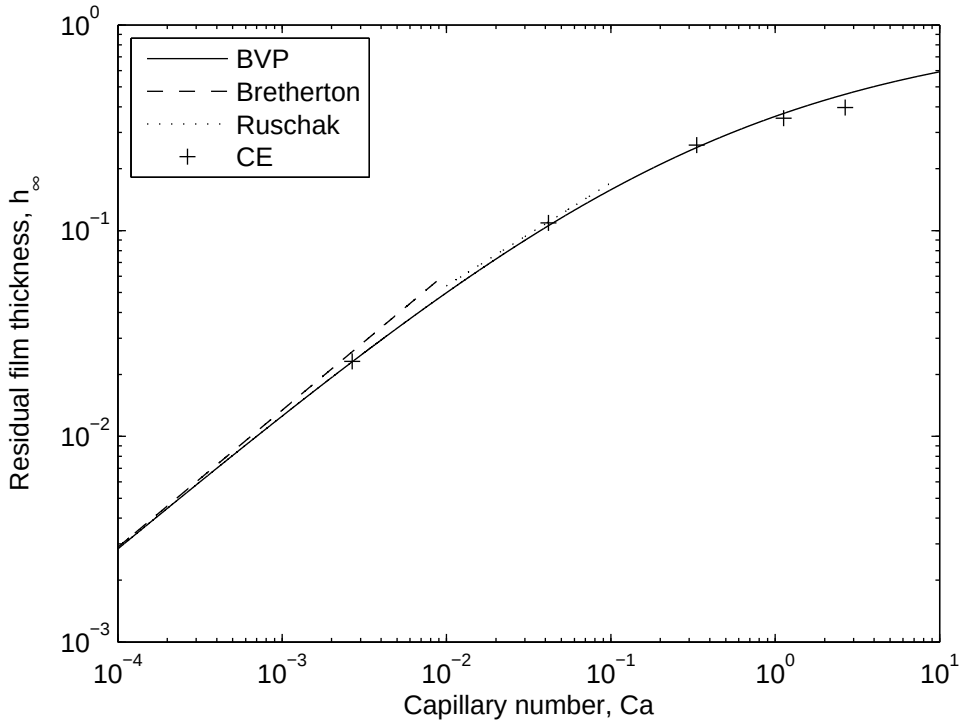

Figure 3: Newtonian residual film thickness results as predicted by a range of models, compared against that predicted by the solution of the BVP.

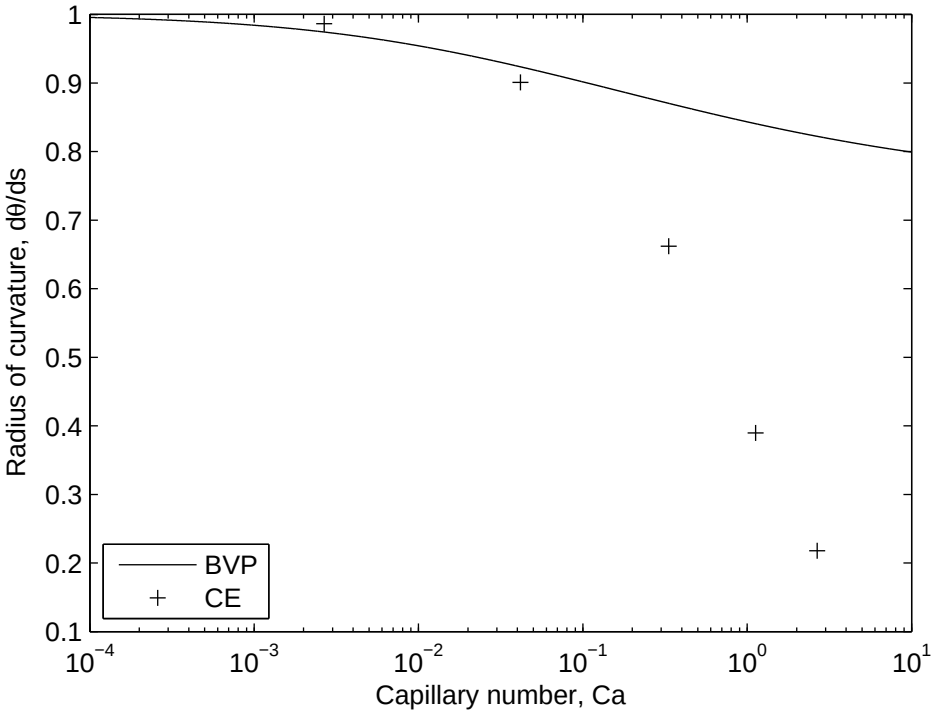

Figure 4: Newtonian radius of curvature results, the radius of curvature having been made non-dimensional by $C - H_\infty$ rather than simply C, allowing easier comparison with Ruschak's equation to be made (for which a constant radius of curvature of unity would be observed).

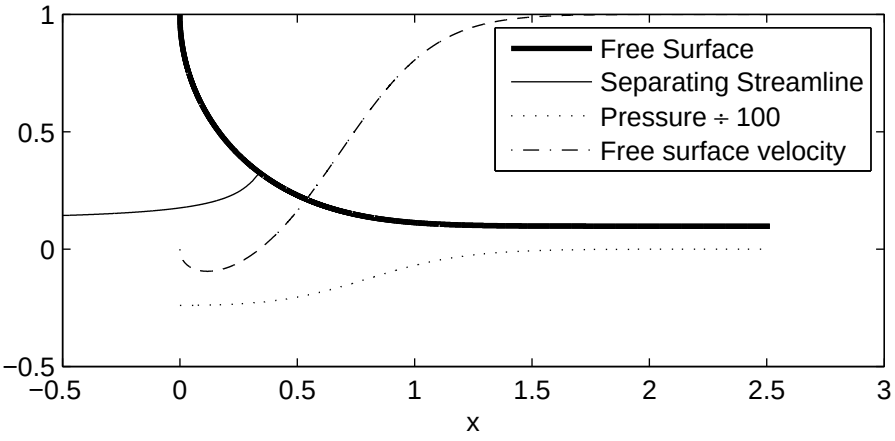

Figure 5: Typical solution for a thin film forming shear thinning liquid, $Ca_P = 0.05, n = 0.75$.

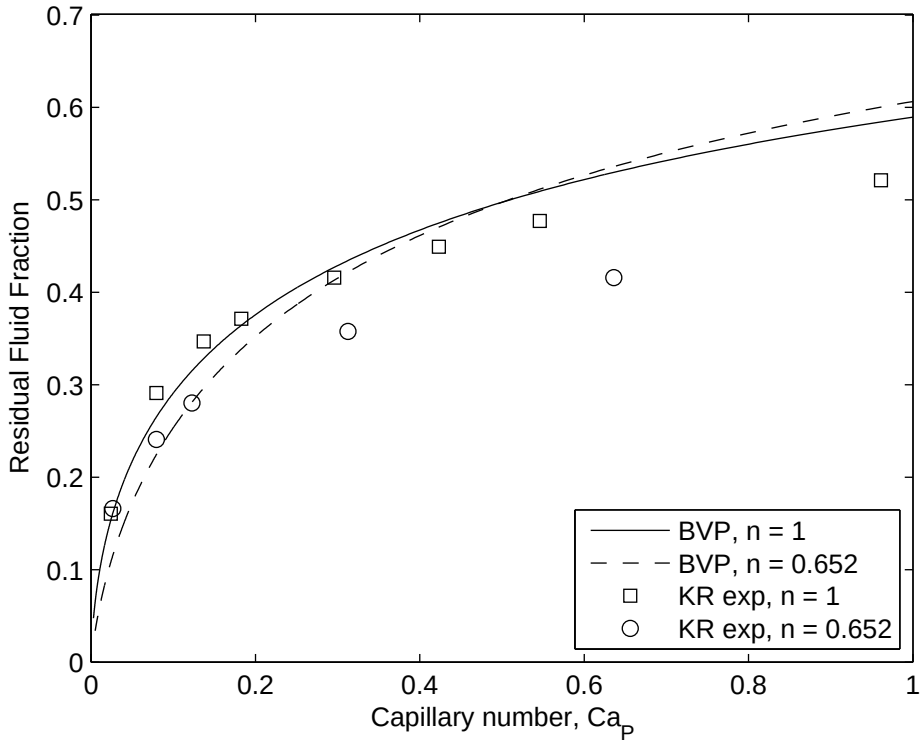

Figure 6: A comparison of prediction against Kamisli & Ryan's [31] experimental residual fluid fraction data for both Newtonian ($n = 1$) and shear thinning ($n = 0.652$) liquids.

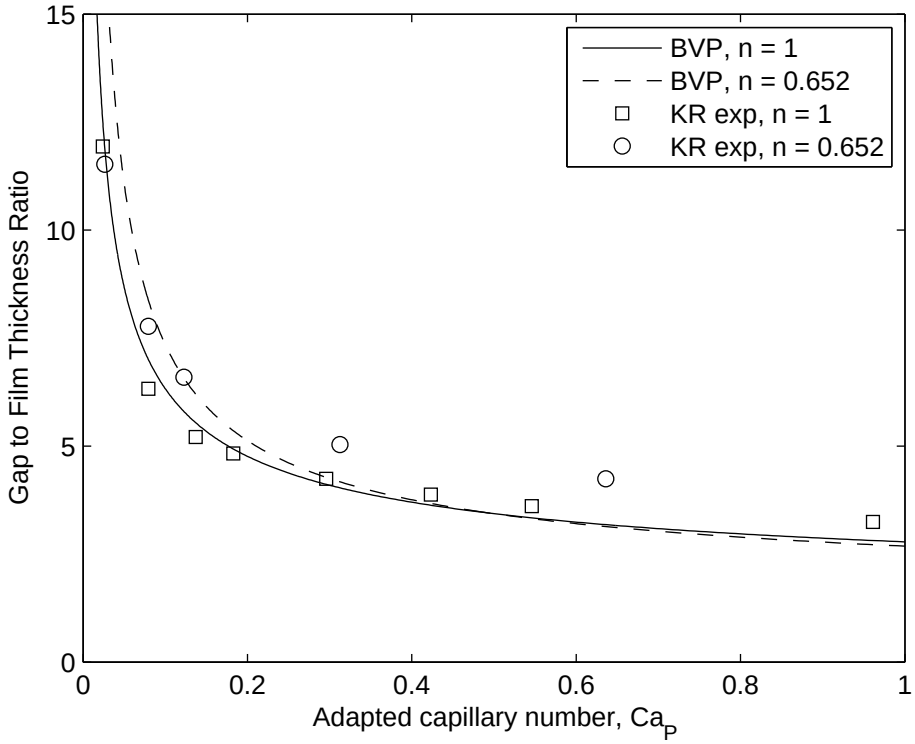

Figure 7: A comparison of prediction against Kamisli & Ryan's [31] experimental gap to film thickness data for both Newtonian ($n = 1$) and shear thinning ($n = 0.652$) liquids.

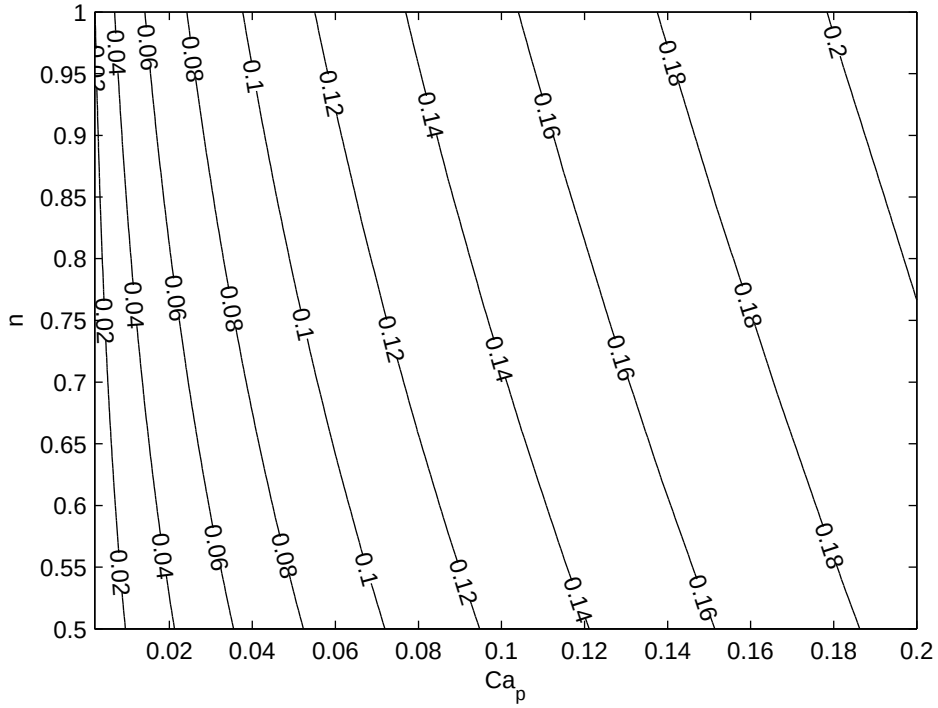

Figure 8: Power law liquids; film thickness contours obtained for $n \in (0.5, 1)$ plotted against $Ca_p \in (0.002, 0.2)$.

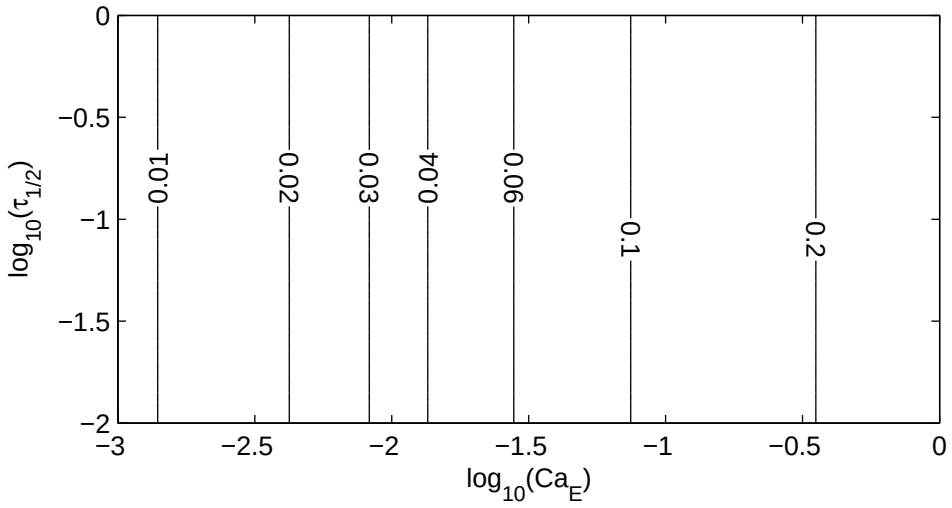

(a) $\alpha = 1.0$

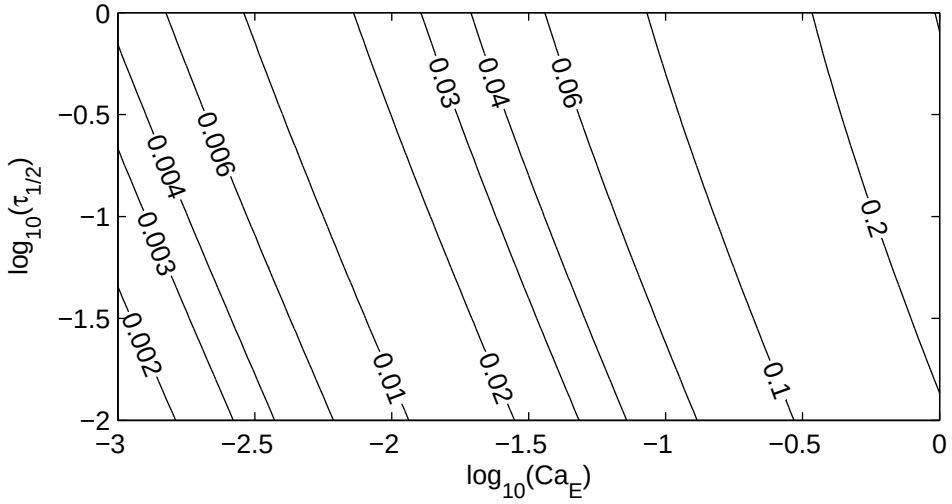

(b) $\alpha = 1.5$

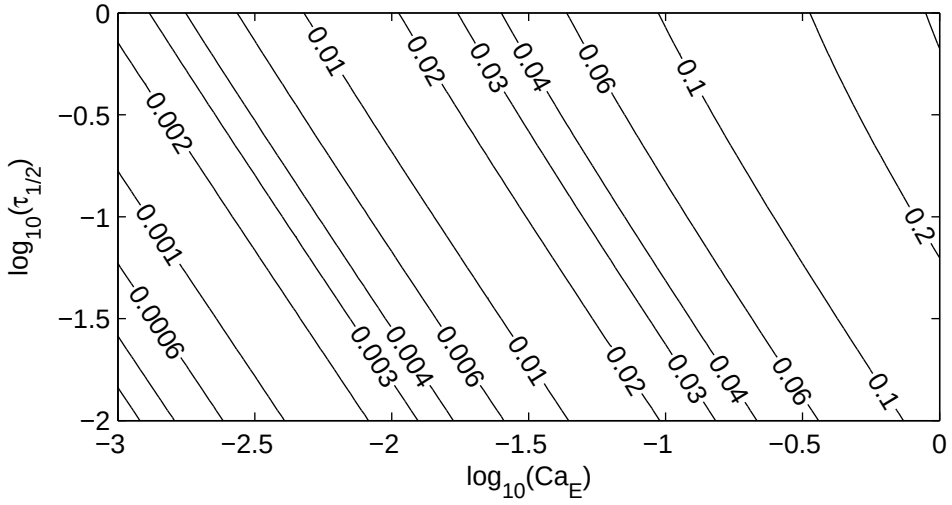

(c) $\alpha = 2.0$

Figure 9: Ellis liquids: film thickness contours obtained for $\log_{10} \tau_{\frac{1}{2}} \in (-2, 0)$ plotted against $\log_{10} Ca_E \in (-3, 0)$ and at three different values of α; α (and hence shear thinning effect) increasing from top to bottom.

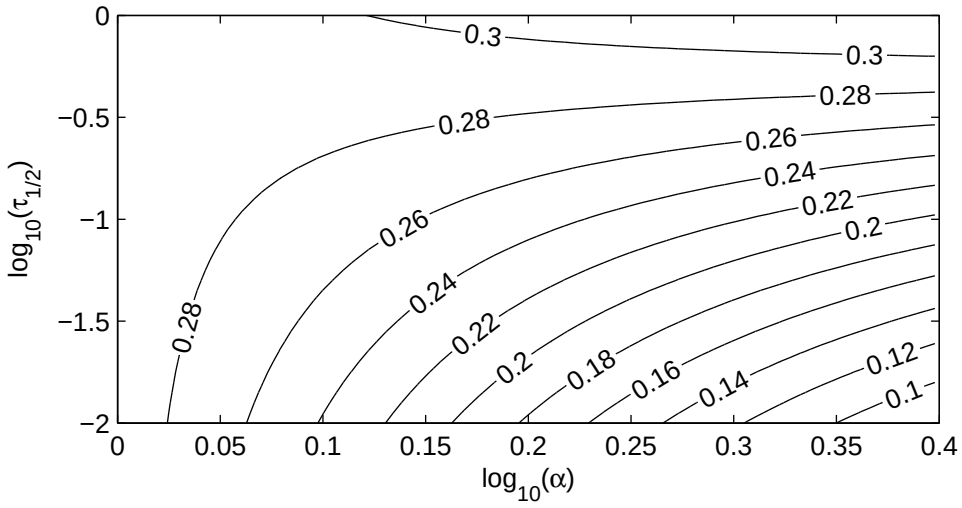

(a) $Ca_E = 1.00$

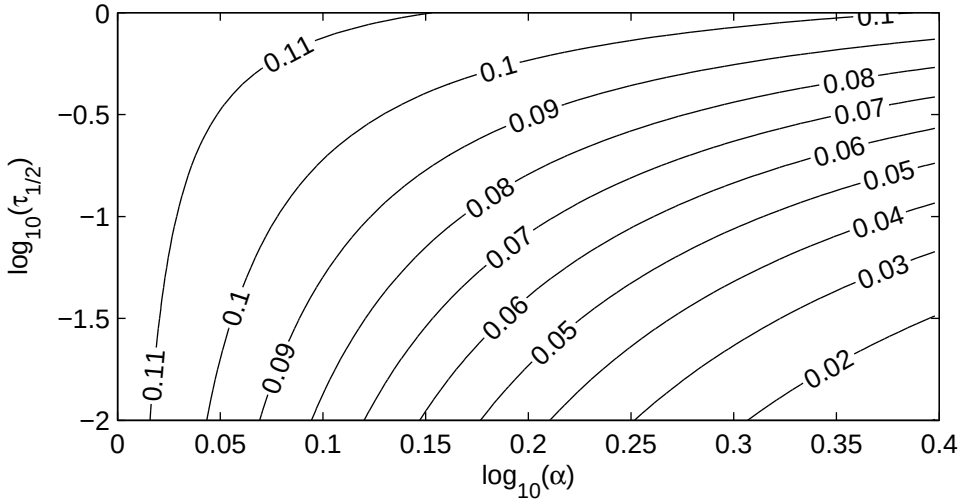

(b) $Ca_E = 0.10$

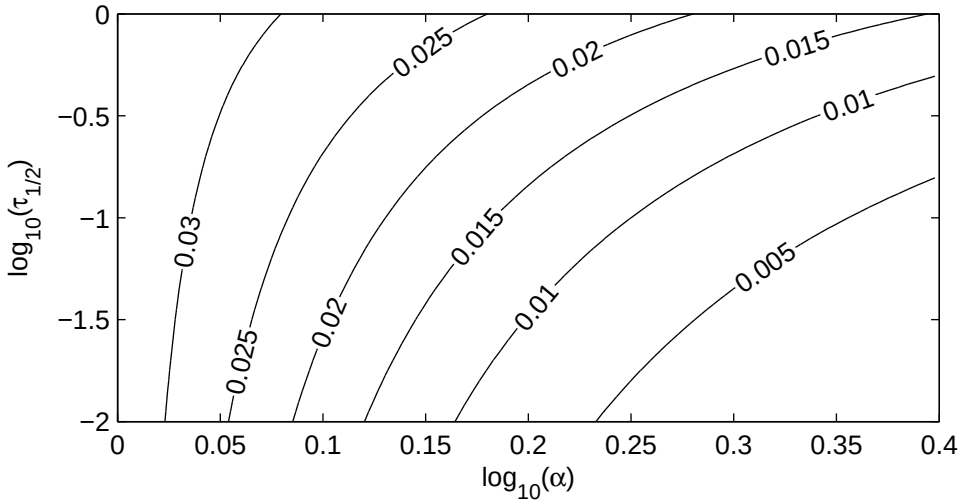

(c) $Ca_E = 0.01$

Figure 10: Ellis liquids: film thickness contours obtained for $\log_{10} \tau_{\frac{1}{2}} \in (-2, 0)$ plotted against $\log_{10} \alpha \in (0, 0.4)$ and at three different values of Ca_E; Ca_E increasing from top to bottom.